Dyes and Pigments 147 (2017) 67–74

Contents lists available at ScienceDirect

Dyes and Pigments

journal homepage: www.elsevier.com/locate/dyepig

A novel synthetic approach to tyrosine dimers based on pterin photosensitization

Lara O. Reid [a], Carolina Castaño [a], M. Laura Dántola [a], Virginie Lhiaubet-Vallet [b], Miguel A. Miranda [b], M. Luisa Marin [b, **], Andrés H. Thomas [a, *]

[a] Instituto de Investigaciones Fisicoquímicas Teóricas y Aplicadas (INIFTA), Departamento de Química, Facultad de Ciencias Exactas, Universidad Nacional de La Plata, CCT La Plata-CONICET, Casilla de Correo 16, Sucursal 4, 1900 La Plata, Argentina
[b] Instituto de Tecnología Química, Universitat Politècnica de València - Consejo Superior de Investigaciones Científicas, Avenida de los Naranjos s/n, 46022 Valencia, Spain

ARTICLE INFO

Article history:
Received 19 May 2017
Received in revised form
6 July 2017
Accepted 24 July 2017
Available online 26 July 2017

Keywords:
Dityrosine
Oxidation
Cross-linking
Pterin
Photocatalyzed synthesis
Photoinduced electron transfer

ABSTRACT

Oxidative damage to proteins leads to a variety of modifications that are markers of pathogenesis. One of the most important modifications is the dityrosine (Tyr_2) cross-link, resulting from an oxidative covalent bond between two tyrosines (Tyr). An optimized methodology for preparation of pure Tyr_2 is important to investigate in detail its physicochemical properties and reactivity. Pterin (Ptr), the parent and unsubstituted compound of oxidized pterins, is able to photosensitize the cross-linking of free tyrosine (Tyr) and tyrosine residues of peptides and proteins through a photoinduced electron transfer mechanism. We have optimized a simple, one-step photocatalyzed formation of Tyr_2, using Ptr as photocatalyst. Our procedure is carried out in aqueous solutions under UV-A radiation for few minutes. The purification of Tyr_2 is performed by reverse-phase chromatography. The obtained highly pure solution is used to fully characterize the Tyr_2 (exact mass and ^1H, ^1H-^1H COSY; DEPT; HSQC and HMBC NMR experiments) and to deeper study its fluorescence properties.

1. Introduction

Oxidative damage to proteins leads to a variety of modifications that are markers of pathogenesis [1]. One of the most important modifications is the dityrosine cross-link, resulting from an oxidative covalent bond between two tyrosines (Tyr), which is involved in amyloid fibril formation, Parkinson's disease or epidermoid carcinoma [2]. Surprisingly, the mechanism of the dityrosine adducts (Tyr_2) formation has been little addressed. On the basis of electronic paramagnetic resonance spectroscopy (EPR), it has been proposed that the process starts with the one-electron oxidation of Tyr, which leads to the long-lived tyrosyl radical (Tyr(-H)$^\bullet$). The coupling of two Tyr(-H)$^\bullet$ yields the dimer o,o′-dityrosine (Tyr_2) as the main product [3] (Fig. 1). This linkage can occur intramolecularly between two Tyr residues in the protein, or intermolecularly between two different protein molecules [4,5]. The latter process leads to products of higher molecular weight and affects the solubility and elastic properties of proteins [6].

An optimized methodology for preparation of pure Tyr_2 is important to investigate in detail its physicochemical properties and reactivity. Aryl-aryl coupling reactions have traditionally been carried out using aryl halides or aryl boronic derivatives as starting materials that eventually are reduced in the presence of metal catalysts such as Pd, Cu or Ni [7]. In fact, Tyr_2 has been prepared from 3-iodo-L-tyrosine through a Miyaura-borylation-Suzuki-coupling reaction in four steps [8]. On the other hand, efforts have been devoted to synthesize Tyr_2 by using a battery of oxidizing agents, but these attempts remain of limited applicability [9–11]. By contrast, *in vitro* oxidation of Tyr with peroxidase and hydrogen peroxide has been shown to be an interesting method for production of Tyr_2 [12–14]. However, the main drawback relies on the isolation of pure Tyr_2 from the incubation mixture, which is not straightforward and requires many steps. Despite of that, this method is still the main way to obtain Tyr_2 and although it has been improved, the purification step is still laborious [15].

More recently, an increasing interest in using light for synthetic organic purposes has been observed. For instance, Boguta and

* Corresponding author. C. C. 16, Sucursal 4, B1904DPI, La Plata, Argentina.
** Corresponding author. Avenida de los Naranjos s/n, 46022, Valencia, Spain.
E-mail addresses: marmarin@qim.upv.es (M. Luisa Marin), athomas@inifta.unlp.edu.ar (A.H. Thomas).

http://dx.doi.org/10.1016/j.dyepig.2017.07.058
0143-7208/

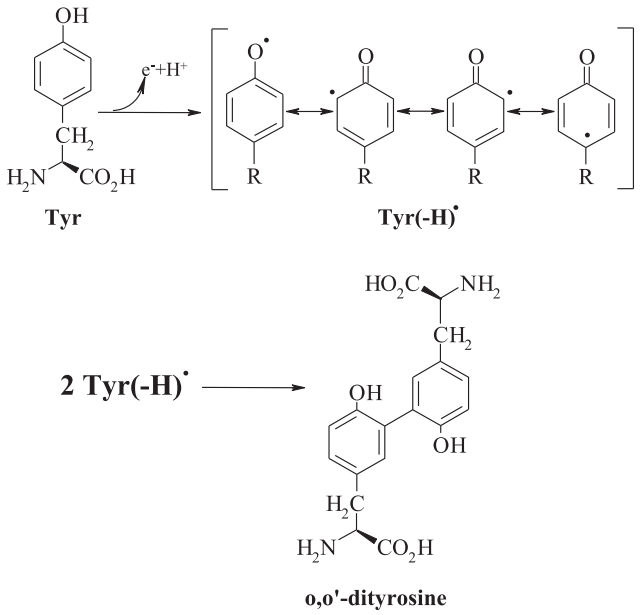

Fig. 1. Postulated oxidative formation of dimer o,o′-dityrosine (Tyr_2).

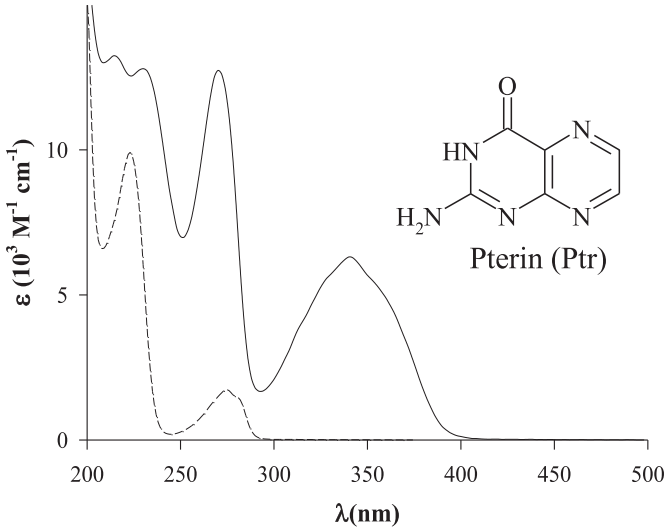

Fig. 2. Absorption spectra of pterin (Ptr, solid line) and tyrosine (Tyr, dashed line) in air-equilibrated aqueous solutions at pH 5.5. Inset: molecular structure of Ptr.

Dancewicz have shown that radiation can induce the dimerization of Tyr by direct light absorption [16,17]. Furthermore, examples of photoredox catalysis applied to a great variety of organic transformations using transition-metal or more convenient metal-free photocatalysts have attributed attention of researchers and examples in literature are countless [18–20].

Interestingly, aryl-aryl bond formation can be triggered through a photocatalyzed oxidation reaction, as reported for the cross-linking of free Tyr and tyrosyl groups in proteins in reaction photosensitized by riboflavin (Rb) [3,21]. In this case, the proposed mechanism was the reduction of the triplet excited state of Rb by Tyr, yielding the Rb radical anion ($Rb^{\bullet -}$) and the tyrosine radical cation ($Tyr^{\bullet +}$), which deprotonates to $Tyr(-H)^{\bullet}$; subsequent dimerization of two $Tyr(-H)^{\bullet}$ gives rise to the formation of Tyr_2.

In this context, pterins appeared to be of particular interest. They are a family of heterocyclic compounds present in a wide variety of living systems and participate in relevant biological functions [22,23]. In addition, these endogenous compounds exhibit an absorption in the UVA region of the solar spectrum (Fig. 2), and thus might represent intrinsic photosensitizers of proteins. Indeed, several studies have demonstrated that pterin (Ptr), the parent and unsubstituted compound of oxidized pterins (Fig. 2), is able to photosensitize the cross-linking of free tyrosine (Tyr) [24] and tyrosine residues of peptides [25,26] and proteins [27–29] through a photoinduced electron transfer mechanism.

2. Material and methods

2.1. General

Pterin (Ptr, purity > 99%, Schircks Laboratories, Switzerland) and tyrosine (Tyr, purity > 99%, Sigma Chemical Co) were used without further purification after checking for impurities by HPLC. Ammonium acetate (NH_4Ac), formic acid (HCOOH) and D_2O were purchased from Sigma Chemical Co. Quinine hemisulfate salt monohydrate and acetonitrile (ACN) were purchased from Fluka and J. T. Baker, respectively.

Electronic absorption spectra were recorded on a Shimadzu UV-1800 spectrophotometer, using quartz cells of 1 cm optical path length. The pH measurements were performed using a pH-meter sensION + pH31 GLP combined with a pH electrode 5010T (Hach) or microelectrode XC161 (Radiometer Analytical). The pH of the aqueous solutions was adjusted by adding drops of HCl and NaOH solutions from a micropipette. The concentration of the acid and the base used for this purpose ranged from 0.1 M to 2 M. Nitrogen and oxygen-saturated solutions were obtained by bubbling for 20 min with these gases (Linde, purity 99.998%), previously saturated in water.

2.2. Steady-state irradiation

The continuous irradiation of the samples, air equilibrated aqueous solutions containing Ptr and Tyr in the pH range 6.0 ± 0.1, was carried out at room temperature. Two different irradiation systems were employed: (I) the sample (1 mL) in quartz cell (1 cm optical path length) was irradiated with a Rayonet RPR 3500 lamp (Southern N. E. Ultraviolet Co.) with emission centered at 350 nm [bandwidth (full width at half-maximum) of ~20 nm], the distance between the lamp and the sample was 4 mm; (II) the sample (100 mL) in a round flask was irradiated in a multilamp photoreactor equipped with 12 lamps (Osram Sylvania, F15T8/BLB) emitting from 310 to 410 nm with a maximal output (1 mW/cm^2) at *ca.* 360 nm.

2.3. High-performance liquid chromatography (HPLC)

2.3.1. Equipment 1 (HPLC1)

A Prominence equipment from Shimadzu (solvent delivery module LC-20AT, on-line degasser DGU-20A5, communications bus module CBM-20, auto sampler SIL-20A HT, column oven CTO-10AS VP, photodiode array (PDA) detector SPD-M20A and fluorescence (FL) detector RF-20A) was employed for monitoring the photochemical processes and to purified the Tyr_2 sample. A Synergi Polar-RP column (ether-linked phenyl phase with polar endcapping, 150 × 4.6 mm, 4 μm, Phenomenex) was used for isolation of Tyr_2 from HPLC runs (preparative HPLC), by collecting the mobile phase after passing though the PDA detector. Solutions containing 100% NH_4Ac (1 mM, pH 6.0 ± 0.1) were used as mobile phase. The same column and runs conditions were used to analyze the purity of the isolated Tyr_2 sample.

2.3.2. Equipment 2 (HPLC2)

Isolation of Tyr_2 was performed on a ProStar equipment from Varian (solvent delivery system model 240, rheodyne injector and PDA detector model 330). A Synergi Polar-RP column (250 × 10 mm, 4 μm, Phenomenex) was used with aqueous solutions of HCl (pH 3.0 ± 0.1) as mobile phase.

2.4. Mass spectrometry analysis

The liquid chromatography mass spectrometry system was equipped with an UPLC chromatograph (ACQUITY UPLC from Waters) coupled to a quadrupole time-of-flight mass spectrometer (Xevo G2-QTof-MS from Waters) (UPLC-QTof-MS). UPLC analyses were performed using the Acquity UPLC BEH Phenyl (1.7 μm, 2.1 × 50 mm) column (Waters). An isocratic elution with 99% of aqueous HCOOH (0.1% v/v) and 1% of ACN was used as mobile phase with a flow rate of 0.2 mL min^{-1}. Mass chromatograms, *i.e.* representations of mass spectrometry data as chromatograms (the *x*-axis representing time and the *y*-axis signal intensity), were registered using different scan ranges. The mass spectrometer was operated in both positive (ESI^+) and negative (ESI^-) ion modes. When solutions of pure Tyr_2 were analyzed, the signals corresponding to the intact molecular ion of Tyr_2 as $[2Tyr\text{-}2H + H]^+$ and $[2Tyr\text{-}2H\text{-}H]^-$ species at *m*/*z* 361 Da and 359 Da, respectively, were observed. However, the resolution was much better in ESI^- than in ESI^+ mode. Therefore the results presented in this work correspond to mass spectrometry analysis carried out in ESI^- mode.

2.5. Nuclear magnetic resonance spectroscopy

The experiments were acquired on a Bruker AV (400 MHz) spectrometer, equipped with a BBI probe. The signal of the solvent, D_2O, was used as a reference for the determination of the chemical shifts (δ) in ppm. When the ^1H was run with suppression of solvent the reference was taken internally by the equipment. ^1H-^1H COSY; DEPT; heteronuclear single quantum correlation experiments (HSQC) and heteronuclear multiple-bond correlation spectroscopy (HMBC) experiments were performed to complete the assignment.

2.6. Determination of the pK_a

The pK_a value of Tyr_2 was determined by UV/Vis-spectrophotometric analysis at room temperature. The experimentally determined absorbance (A) at a given wavelength can be fitted by equation (1)

$$A = (c \cdot l) \cdot \left(\varepsilon_a\left[H^+\right] + \varepsilon_b K_a\right) \Big/ \left(K_a + \left[H^+\right]\right) \quad (1)$$

where ε_a and ε_b are the molar absorption coefficients of the acid and basic forms of Tyr_2 respectively, c is the total concentration of the species involved in the acid–base equilibrium (*ie.* $[Tyr_2]$), l is the optical path length and K_a is the dissociation constant of the acid form of the species involved in the acid–base equilibrium. UV-visible absorption spectra were registered on the above-mentioned spectrophotometer. A more-detailed description of pK_a determinations has been given elsewhere [30].

2.7. Fluorescence spectroscopy

Fluorescence measurements were performed at room temperature using a single-photon-counting equipment FL3 TCSPC-SP (Horiba Jobin Yvon).

2.7.1. Steady-state experiments

The sample solution in a quartz cell was irradiated with a CW 450 W Xenon source through an excitation monochromator (FL-1004). The luminescence, after passing through an emission monochromator (iHR320), was registered at 90° with respect to the incident beam using a room-temperature R928P detector. The emission measurements were performed at 25 °C. Corrected fluorescence spectra obtained by excitation at 280 and 315 nm were recorded in the ranges 310–550 nm and 340–550 nm, respectively. The excitation spectra were recorded between 260 and 380 nm, monitoring the fluorescence intensity at 410 nm.

The fluorescence quantum yields (Φ_F) were determined from the corrected fluorescence spectra using the following equation:

$$\Phi_F = \Phi_F^R \frac{I}{I^R}\frac{A^R}{A} \quad (2)$$

where I is the integrated intensity, A is the absorbance at the excitation wavelength and the superscript R refers to the reference fluorophore. In our experiments, quinine hemisulfate in 0.5 M H_2SO_4 was used as a reference [31] ($\Phi_F = 0.546$ [32]). The sample and reference were excited at the same wavelength. To avoid inner filter effects, the absorbance of the solutions at the excitation wavelength was kept below 0.10.

2.7.2. Time-resolved experiments

NanoLED sources (maxima at 295 and 341 nm) were used for excitation. The emitted photons, after passing through the iHR320 monochromator, were detected by a TBX-04 detector connected to a TBX-PS power supply and counted by a FluoroHub-B module, controlled using the DataStation measurement control software application. The selected counting time window for the measurements reported in this study was 0–200 ns.

In addition, the time-resolved emission spectra (TRES) of solutions were obtained, measuring the decay curves at multiple emission wavelengths to construct a 3D data set of counts *versus* time and *versus* wavelength. The Global Analysis of TRES, a fit calculation (up to 5 exponentials) performed globally on up to 100 separate decay curves, was carried out using the DAS6 Fluorescence Decay Analysis software.

2.8. Laser flash photolysis

A pulsed Nd:YAG laser (Lotis TII) was used for the excitation at 355 nm. The single pulses were of *ca.* 10 ns duration and the energy was 21 mJ/pulse. A pulsed Xenon lamp was employed as detecting light source. The laser flash photolysis apparatus consisted of the pulsed laser, the Xe lamp, a monochromator, and a photomultiplier made up of a tube, housing, and power supply. The output signal from the oscilloscope was transferred to a personal computer. All transient spectra were recorded using 1 × 1 cm^2 quartz cells with 4 mL capacity, and solutions were bubbled for 20 min with N_2 before acquisition. Aqueous solutions of 75 μM Ptr ($A_{355} = 0.4$) were prepared in acidic water at pH = 5. For quenching experiments, stock solutions of quenchers were prepared so that it was only necessary to add microliter volumes to the sample cell to obtain appropriate concentrations of the quencher.

3. Results and discussion

3.1. Mechanistic study of the photoreaction between Ptr and Tyr

Up to now, few data are available on the process responsible for Tyr dimerization as a result of a photocatalyzed process. A type I mechanism involving a photoinduced electron transfer from the

amino acid to the triplet excited state of the photosensitizer ($^3Phs^*$) has been proposed for Rb and Ptr [3,21,24]. Briefly, after the excitation of the Phs and formation of its triplet excited state, $^3Phs^*$ (Reactions (3) and (4)), the one electron oxidation of Tyr takes place leading to the formation of the corresponding pair of radical ions, $Phs^{\bullet-}$ and $Tyr^{\bullet+}$ (Reaction (5)), that may deprotonate to Tyr(-H)$^\bullet$ (Reaction (6)) (Fig. 1). The electron transfer from $Phs^{\bullet-}$ to O_2 regenerates Phs and forms $O_2^{\bullet-}$ (Reaction (7)), which, in turn, disproportionates to form H_2O_2 (Reaction (8)). Finally a group of processes, represented schematically by Reaction (9), leads to the oxidation of Tyr and consumption of O_2. Alternatively, Tyr(-H)$^\bullet$ suffers dimerization to yield Tyr_2 (Reaction (10), Fig. 1) (*vide infra*).

$$Phs \rightarrow {}^1Phs^* \quad (3)$$

$${}^1Phs^* \xrightarrow{ISC} {}^3Phs^* \quad (4)$$

$${}^3Phs^* + Tyr \rightarrow Phs^{\bullet-} + Tyr^{\bullet+} \quad (5)$$

$$Tyr^{\bullet+} \rightarrow Tyr(-H)^\bullet + H^+ \quad (6)$$

$$Phs^{\bullet-} + O_2 \rightarrow Phs + O_2^{\bullet-} \quad (7)$$

$$2H^+ + 2O_2^{\bullet-} \rightarrow H_2O_2 + O_2 \quad (8)$$

$$Tyr^{\bullet+} \Big/ Tyr(-H)^\bullet + O_2 \rightarrow Tyr(ox) \quad (9)$$

$$2Tyr(-H)^\bullet \rightarrow Tyr_2 \quad (10)$$

However, the involved excited states and/or radical species of Reactions (5) and (6) have never been detected spectroscopically in the case of Ptr. In this context, nanosecond laser flash photolysis at 355 nm (Nd:YAG laser) of Ptr in the presence of Tyr was performed. The transient absorption spectrum of N_2 flushed Ptr solution (75 μM) in acidic water at pH = 5 showed a band with a maximum at around 430 nm (Fig. 3, black triangles), which decayed by a biexponential process with lifetimes of τ_1 and τ_2 of 0.34 and 3.8 μs, respectively. This result is in agreement with the data described in the literature for the triplet-triplet transient absorption of Ptr [33]. Addition of increasing amounts of Tyr (up to 500 μM) resulted in a shortening of τ_2. It should be mentioned that the employed experimental set up does not allow to detect changes of the sub μs lifetime τ_1. The bimolecular quenching rate constant (k_q) was determined by means of the Stern-Volmer plot (Fig. 3) following Equation (11):

$$1/\tau = 1/\tau_2 + k_q[Tyr] \quad (11)$$

where τ_2 and τ are the triplet lifetimes (in s) in the absence and in the presence of Tyr, respectively, and [Tyr] is the concentration of the amino acid in M. An efficient quenching was observed with a k_q of *ca.* 2×10^9 M^{-1} s^{-1}. This k_q, close to water diffusion controlled rate constant [34], points toward a possible electron transfer mediated by the triplet excited state of Ptr.

Accordingly, the transient absorption spectrum in the presence of Tyr showed two new bands: a sharp one at *ca* 410 nm and a broader one (400–550 nm) (Fig. 3, white triangles). On the basis of literature data, the former could be satisfactorily correlated with the known spectral properties of the tyrosyl radical (Tyr(-H)$^\bullet$) obtained after deprotonation of the $Tyr^{\bullet+}$, which has been reported peaking at 410 nm [35]. The latter, as stated in Reaction (5), should thus be due to the radical anion of Ptr ($Ptr^{\bullet-}$). This species was

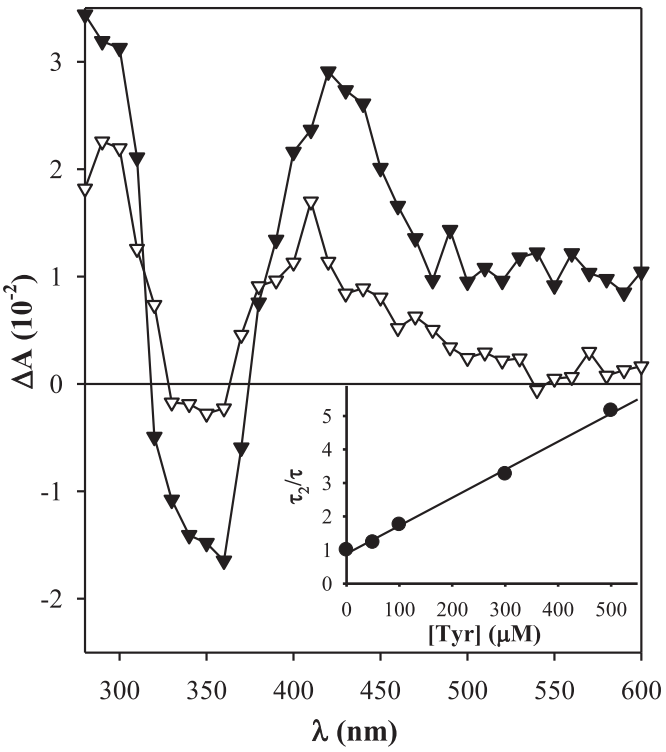

Fig. 3. Transient absorption spectra of N_2 flushed aqueous solution of Ptr (75 μM) at pH 5 in the absence (black triangle, 0.4 μs after the laser pulse) or in the presence of 500 μM Tyr (white triangle, 15 μs after the laser pulse). Inset: corresponding Stern-Volmer plot.

further assigned by exciting Ptr in the presence of DABCO, used as reductant. The $^3Ptr^*$ was efficiently quenched in the presence of DABCO giving rise to the formation of a new band (Fig. 4) that is coincident with the broad absorption species observed at 400–550 nm in the presence of Tyr (Fig. 3).

Moreover, the thermodynamic feasibility of the electron transfer between Tyr and $^3Ptr^*$ was determined using the Gibbs energy of photoinduced electron transfer Equation (12):

$$\Delta G = E^\circ\left(Tyr^{\bullet+}\Big/Tyr\right) - E^\circ\left(Ptr\Big/Ptr^{\bullet-}\right) - E_T(Ptr) \quad (12)$$

where $E^\circ(Tyr^{\bullet+}/Tyr)$ is the reduction potential of Tyr (*ca.* 0.93 V vs NHE) [36], $E^\circ(Ptr/Ptr^{\bullet-})$ is the reduction potential of Ptr (*ca.* −0.55 V vs NHE) and $E_T(Ptr)$ is the triplet excited state energy of Ptr (*ca.* 2.52 eV) [37]. A value of $\Delta G = -1.04$ eV was obtained, supporting the occurrence of a photoinduced electron transfer between $^3Ptr^*$ and Tyr, leading to the tyrosyl radical Tyr(-H)$^\bullet$, which in turn could dimerize to give rise to Tyr_2.

3.2. Preparation of Tyr_2

Then, acidic air-equilibrated aqueous solutions of Tyr were exposed to UV-A radiation in the presence of Ptr. Under these experimental conditions only Ptr is selectively excited, as it can be inferred from the corresponding absorption spectra (Fig. 2). The photocatalyzed reaction was run in quartz cells of 1.0 cm optical path length and the photomixtures were analyzed by reverse-phase chromatography employing the equipment HPLC1, using a C18 column and aqueous solution of NH_4Ac 1 mM (pH 6.0) as eluent (see Material and Methods). The concentration profiles of Ptr and Tyr, determined by UV-Vis chromatograms, showed a decrease of the Tyr concentration as a function of irradiation time, whereas the

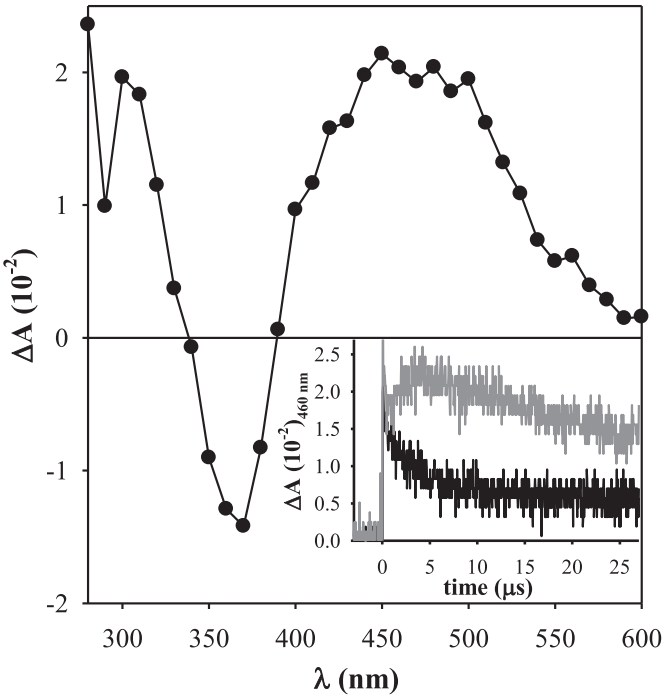

Fig. 4. Transient absorption spectrum of N_2 flushed aqueous solution of Ptr (75 μM) at pH 5 in the presence of 1 mM DABCO (5.4 μs after the laser pulse). Inset: Time dependence of the absorbance at 460 nm at 0 (black line) and 1 mM (gray line) of DABCO.

Ptr concentration did not change in the analyzed time-window (Fig. 5). However, a new peak at 6.45 min was differentiated from the other products taking advantage of its particular emission features [15]. Therefore, fluorescence chromatograms of irradiated solutions (excitation at 280 nm and emission at 410 nm) were recorded and only one significant peak was detected at the same retention time (t_R) (Fig. 5b). The absorption and emission spectra of this new peak are red-shifted with respect to those of Tyr [38]. The absorption spectrum of this product, registered by the UV-Vis detector (see inset of Fig. 5a), corresponded to the previously reported for the acidic form of Tyr_2 [39,40]. Therefore, this new peak was safely assigned to the dimeric form of Tyr (Tyr_2). As shown in the inset of Fig. 5b, the production of Tyr_2 increased with irradiation time reaching a maximum and then decreased slowly.

To optimize the production of Tyr_2, the concentration profiles of this product were obtained at different concentrations of each reactant, taking into account the solubility limitations. In all cases, the area of the peak corresponding to Tyr_2 increased with irradiation time reaching a maximum (Fig. 5). This analysis revealed that the highest concentration of Tyr_2 was obtained when a solution containing 500 μM of Tyr and 100 μM of Ptr was irradiated 10 min with UVA light (irradiation system I, Material and Methods).

3.3. Isolation and identification of Tyr_2

Upon applying the optimized experimental conditions to maximize the production of Tyr_2, the compound was isolated from HPLC runs by collecting the mobile phase after passing through the HPLC1-PDA detector. The analysis of the collected fraction showed only one peak with spectroscopic features corresponding to that of Tyr_2 (Fig. S1, Supporting Information), suggesting that the isolation of Tyr_2 was done successfully.

To unequivocally characterize the isolated Tyr_2, first it was analyzed by UPLC coupled to ESI mass spectrometry (UPLC-MS)

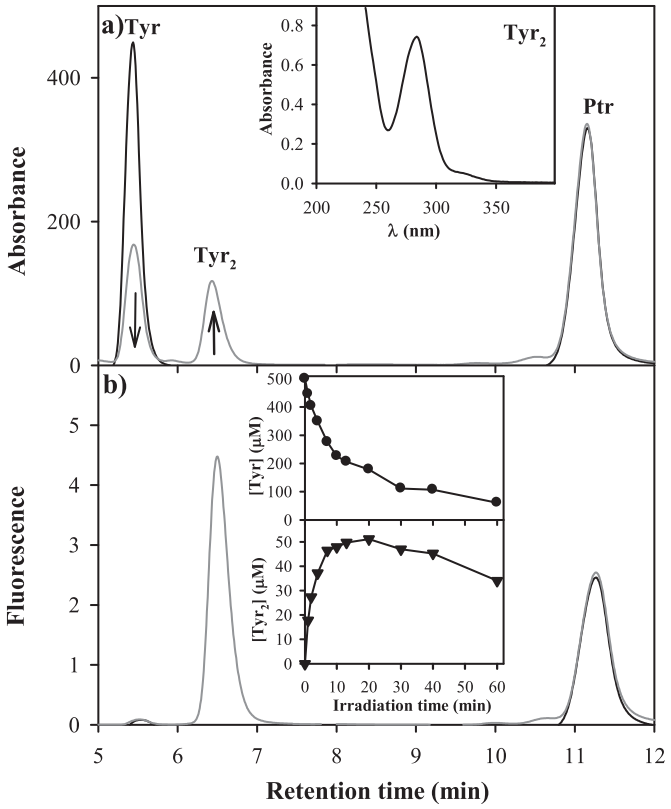

Fig. 5. Chromatograms, obtained using a) the HPLC1-PDA detector at 280 nm and b) HPLC1-FL detector (excitation at 280 nm, emission at 410 nm), of a solution containing Tyr and Ptr before (black line) and after 10 min (gray line) of irradiation. Inset: a) absorption spectrum of Tyr_2 in NH_4Ac (1 mM, pH = 6.0) obtained for the peak at 6.45 min in the chromatogram; b) evolution of the Tyr and Tyr_2 concentration as a function of irradiation time.$[Ptr]_0$ = 100 μM, $[Tyr]_0$ = 500 μM, pH = 6.0.

(Material and Methods). The corresponding mass chromatograms showed a single peak (Fig. 6) with a *m/z* value of 359.1239 Da which corresponds to $[2Tyr\text{-}2H\text{-}H]^-$. Accordingly, the mass chromatograms registered for the specific ion mass of 359.1239 Da showed

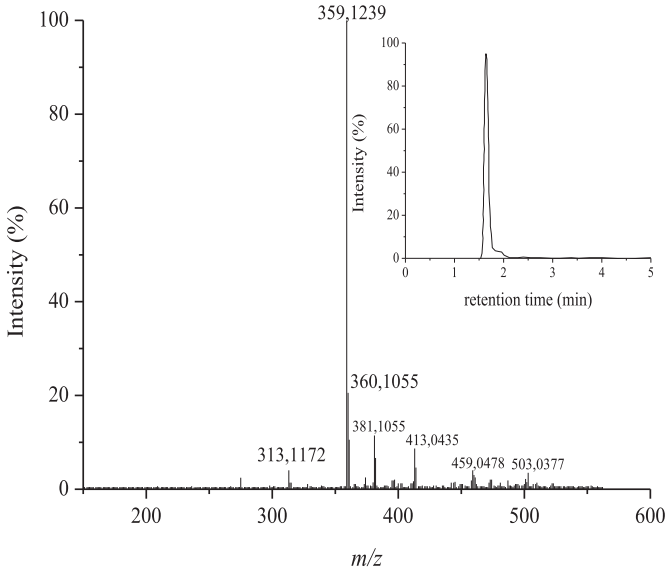

Fig. 6. Mass spectrum obtained from UPLC-QTof-MS analysis of an isolated aqueous solution of Tyr_2 (14 μM). Inset: Mass chromatogram of *m/z* 359.1239 Da. Mode ESI^-, Voltage = 30 V.

that this molecular weight was observed at only one t_R value, indicating that only one isomer of Tyr_2 is formed.

Then, the isolated compound was fully characterized by NMR spectroscopy (Material and Methods). Taking into account that this technique needs a relatively high concentration of the analyte, a 100 mL aqueous solutions of Tyr (500 μM) and Ptr (100 μM) was irradiated using the irradiation system II (Material and Methods) during 10 min. Tyr_2 was isolated using the equipment HPLC2 (Material and Methods), equipped with a semi-preparative C18 column. In addition, to avoid interferences in the subsequent NMR analysis, aqueous solutions of HCl (pH 3.0 ± 0.1) was used as eluent to collect Tyr_2. After that, the solvent was removed by lyophilization.

Initially the ^{1}H NMR was run in slightly acidic D_2O to compare to the previously described Tyr_2. In fact, the spectrum was coincident to the one already described (see Supporting Information, Figs. S2–S8) [9]. However, to fully characterize the dimer, much better resolution was obtained in slightly basic D_2O; therefore all the experiments were carried at pH *ca.* 11 (^{1}H, ^{1}H-^{1}H COSY, DEPT, HSQC and HMBC). Due to the limited solubility of Tyr_2, the quaternary carbons were only identified with the help of HMBC: ^{1}H NMR (400 MHz, basic D_2O) δ = 7.31 (*br* s, 1H), 7.25 (*br* s, 1H), 7.17 (*br* d, J = 8.0 Hz, 1H), 7.04 (*br* d, J = 8.0 Hz, 1H), 6.99 (*br* d, J = 8.0 Hz, 1H), 6.74 (*br* d, J = 8.0 Hz, 1H), 3.45 (dd, J = 8.0, 4.8 Hz, 1H), 3.39 (dd, J = 8.0, 5.3 Hz, 1H), 3.01 (dd, J = 13.2, 4.8 Hz, 1H), 2.92 (dd, J = 13.6, 5.3 Hz, 1H), 2.74 (dd, J = 13.2, 8.0 Hz, 1H), 2.69 (dd, J = 13.6, 8.0 Hz, 1H); ^{13}C NMR (100 MHz, basic D_2O) δ = 40.1 (CH_2), 40.3 (CH_2), 57.6 (2xCH), 119.0 (CH), 121.9 (CH), 129.6 (CH), 129.7 (CH), 129.8 (CH), 131.5 (CH), 152.9 (2xC), 156.9 (2xC), 182.6 (2xC). A parallel set of experiments were carried out for commercial Tyr under basic D_2O in order to compare (see Supporting Information, Figs. S9–S15).

3.4. Determination of the yield

As previously reported, the phenol groups of Tyr_2 are much more acidic than that of Tyr and the two acid-base forms have well differentiated spectral features [13,15], e.g. the absorbance maxima are 283 and 315 nm for the acid and basic form, respectively. Therefore, the absorption spectra of the isolated compound was recorded over a range of pH (Fig. 7) and the corresponding pK_a value was determined to be 7.25 ± 0.02 (Material and Methods), which is in agreement with that published in the literature [40].

The absorbance of the solution of the isolated compound (pH 6.0) at 283 nm was measured, and the concentration of Tyr_2 was determined using the Lambert-Beer law ($A^\lambda = \varepsilon^\lambda_{Tyr2}\, l[Tyr_2]$), using $\varepsilon^{283}_{Tyr2} = (5680 \pm 30)\ M^{-1}cm^{-1}$ for the molar extinction coefficient of the acid form [15]. With this data, the mass of Tyr_2 in the isolated sample was calculated taking into account the volume obtained during the isolation of the sample. The result was compared to the initial mass of Tyr and a value of 9 (±1) % was obtained for the overall yield of the one-step photocatalyzed process.

3.5. Fluorescence properties

As mentioned above, the Tyr_2 is fluorescent and its particular emission properties are used to detect its formation in proteins and peptides [6,15]. Moreover, fluorescence of Tyr_2 is an unspecific marker of oxidative damage in proteins [6,15]. Despite the biological and medical importance of Tyr_2 emission, the reports on fluorescence of isolated Tyr_2 in aqueous solutions are rare [15,39].

The fluorescence spectra of Tyr_2 in acid (pH 4.8 ± 0.1) and alkaline (pH 9.7 ± 0.1) solutions were recorded by excitation at 280 nm and 315 nm, respectively. Both fluorescence spectra were identical, with an emission maximum at 410 nm (Fig. 8). The fluorescence spectrum is unaffected by the pH of the solution

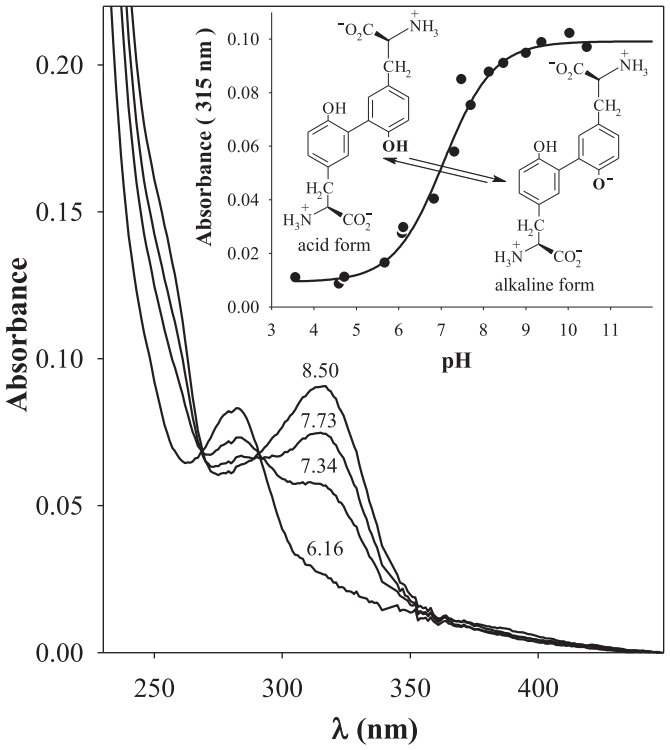

Fig. 7. Absorption spectra of air equilibrated aqueous solution of purified Tyr_2 at different pH values. The pH values appear above each spectrum. Inset: acid-base equilibrium in aqueous solution of Tyr_2 and the variation of the absorbance at 315 nm (circles) as a function of pH; the solid line represents the absorbance calculated by fitting the experimental data to Equation (1). [Tyr_2] = 12 μM.

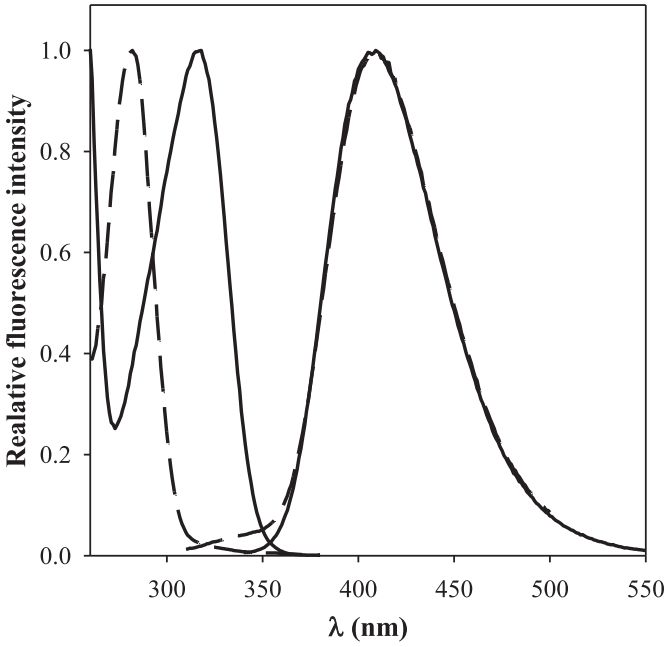

Fig. 8. Normalized emission and excitation spectra of Tyr_2 in acid (dashed line) and alkaline (solid line) aqueous solutions. Emission spectra in acid and alkaline solution were obtained upon excitation at 280 and 315 nm, respectively. Excitation spectrum was obtained at 410 nm.

Table 1
Fluorescence quantum yields (Φ_F) in nitrogen-saturated, air-equilibrated and oxygen-saturated aqueous solutions, fluorescence lifetime (τ_F) and fluorescence maxima (λ_F) of Tyr_2.

Acid- base form	λ_F (nm) (±2)	$\Phi_F(O_2)$	$\Phi_F(N_2)$	Φ_F(Air)	τ_F(ns) (±0.1)
acid	410	0.29(±0.02)	0.29(±0.02)	0.28(±0.02)	4.0
base	410	0.42(±0.02)	0.46(±0.03)	0.46(±0.02)	4.4

because the emitting species is always the singly ionized Tyr_2 chromophore, produced by either ground state (alkaline pH) or excited-state (acid pH) ionization [41]. In contrast, a prominent shift of maximum excitation spectra from 280 to 315 nm on varying the pH from the acid to the alkaline medium was observed (Fig. 8). These results are in good agreement with those published in the literature [6,15].

Then, the fluorescence quantum yields (Φ_F) of the acid and basic forms were determined in oxygen-free, air-equilibrated and oxygen-saturated solutions (Table 1). For each acid-base form, the Φ_F value does not depend on the oxygen concentration, indicating that this species does not quench the singlet excited state.

The Φ_F value of the acid form of Tyr_2 is lower than that of the basic form. This fact suggests that when the acid form is excited not all the singlet excited states undergo deprotonation to yield the basic form. A proportion of them deactivate before ionization. Fig. 8 shows that the fluorescence spectrum of the acid form has a small contribution between 300 and 370 nm, that might be a weak emission of the protonated singlet excited state. The radiationless deactivation of the singlet excited state before deprotonation also could contribute to reduce the Φ_F value, by respect to the Φ_F value of the basic form.

Fluorescence decays were analyzed for acid and base forms of Tyr_2. The emission decays, registered at 410 nm, were clearly monoexponential (Fig. 9) with a value of fluorescence lifetime (τ_F) of 4.0 (±0.1) ns and 4.4 (±0.1) ns, in acid and alkaline media, respectively. These results are in disagreement with previous works, in which biexponential fluorescence decay pattern of Tyr_2 have been reported [39]. We attribute this difference to the purity of our samples using our method of synthesis and isolation. The lower τ_F in acid than in alkaline medium can be explained by the role of protons, which act as quenchers of Tyr_2 fluorescence. The global analysis of TRES data confirmed that only one component is responsible for the fluorescence of the sample.

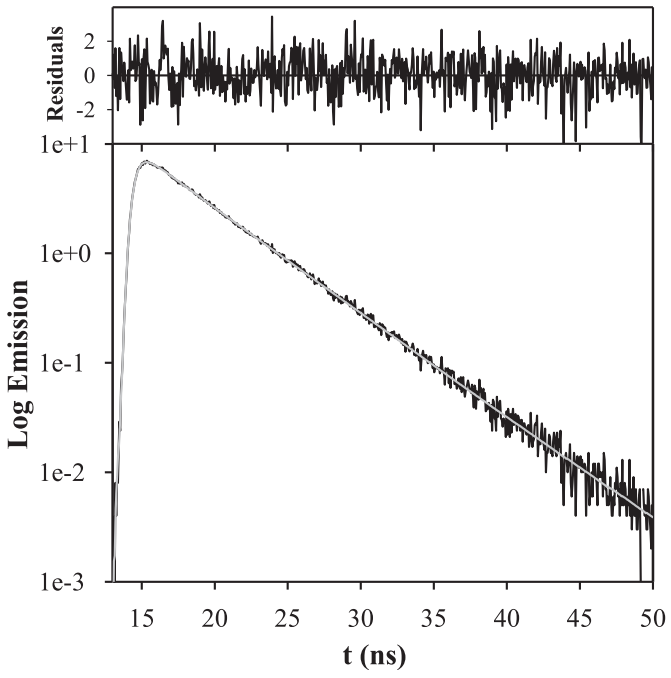

Fig. 9. Fluorescence decays and monoexponential fitting analysis of the Tyr_2 emission in alkaline aqueous solution (17 μM, pH = 9.75, λ_{exc} = 341 nm, λ_{an} = 410 nm).

4. Conclusions

Pterin (Ptr) photoinduce the formation of dimers of tyrosine (Tyr_2). The process is initiated by an electron transfer from tyrosine (Tyr) to the triplet excited state of Ptr, leading to the formation of Tyr radicals that recombine to form Tyr_2. This photochemical process suggests: (i) the potential of Ptr as photocatalyst for aryl-aryl bond formation reactions and, (ii) since pterins are endogenous photosensitizers, they might significantly contribute to the harmful effects of UV-A radiation on the human skin.

We have optimized a simple, one-step photocatalyzed formation of Tyr_2, using Ptr as a photocatalyst. Our procedure is carried out in aqueous solutions under UV-A radiation for few minutes. The purification of Tyr_2 was performed by reverse-phase chromatography. The highly pure obtained solution was used to fully characterize the Tyr_2 (exact mass and ^1H and ^{13}C NMR) and to deeper study its fluorescence properties.

Acknowledgements

The present work was partially supported by Consejo Nacional de Investigaciones Científicas y Técnicas (CONICET; Grant PIP 0304), Agencia de Promoción Científica y Tecnológica (ANPCyT; Grants PICT 2012-0508), and Universidad Nacional de La Plata (UNLP; Grant X586 and X712). L.O.R. and C.C. thanks CONICET for doctoral research fellowships. Funding from the Programa CSIC de Cooperación Científica para el Desarrollo (iCOOPLight project ref 20105CD0017) is gratefully acknowledged. A.H.T. and M.L.D are research members of CONICET. The authors thank Dr. Mariana Vignoni (INIFTA, CONICET) and Nathalie Martins-Froment of the Service Commun de Spectrométrie de Masse (FR2599), Université de Toulouse III (Paul Sabatier) for their crucial contributions in mass spectrometry measurements.

Appendix A. Supplementary data

Supplementary data related to this article can be found at http://dx.doi.org/10.1016/j.dyepig.2017.07.058.

References

[1] Stadtman ER. Implication of protein oxidation in protein turnover, aging, and oxygen toxicity. Basic life Sci 1998;49:331–9.
[2] Balasubramanian D, Kanwar R. Molecular pathology of dityrosine cross-links in proteins: structural and functional analysis of four proteins. Mol Cel Biochem 2002;234/235:27–38.
[3] Dalsgaard TK, Nielsen JH, Brown BE, Stadler N, Davies MJ. Dityrosine, 3,4 dihydroxyphenylalanine (DOPA), and radical formation from tyrosine residues on milk proteins with globular and flexible structures as a result of riboflavin-mediated photo-oxidation. J Agric Food Chem 2011;59:7939–47.
[4] Giulivi C, Davies KJ. Dityrosine: a marker for oxidatively modified proteins and selective proteolysis. Methods Enzymol 1994;233:363–71.
[5] Stadtman ER. Protein oxidation and aging. Science 1992;257:1220–4.
[6] Amado R, Aeschbach R, Neukom H. Dityrosine: in vitro production and characterization. Methods Enzymol 1984;107:377–88.
[7] Hassan J, Sévignon M, Gozzi C, Schulz E, Lemaire M. Aryl–Aryl bond formation one century after the discovery of the ullmann reaction. Chem Rev 2002;102:1359–470.
[8] Hutton CA, Skaff O. A convenient preparation of dityrosine via Miyaura borylation–Suzuki coupling of iodotyrosine derivatives. Tetrahedron Lett 2003;44:4895–8.
[9] Nishiyama S, Kim MH, Yamamura S. Syntheses of isodityrosine, dityrosine and

related compounds by phenolic oxidation of tyrosine and phenylglycine derivatives using an electrochemical method. Tetrahedron Lett 1994;35:8397–400.
[10] Eickhoff H, Jung G, Rieker A. Oxidative phenol coupling—tyrosine dimers and libraries containing tyrosyl peptide dimers. Tetrahedron 2001;57:353–64.
[11] Lee D, Hwang S, Choi JY, Ahn I-S, Lee C-H. A convenient preparation of dityrosine via Mn(III)-mediated oxidation of tyrosine. Process Biochem 2008;43:999–1003.
[12] Gross AJ, Sizer IW. The oxidation of tyramine, tyrosine, and related compounds by peroxidase. J Biol Chem 1959;234:1611–4.
[13] Andersen SO. Acta physio Scand 1966;66:1–81.
[14] Malanik V, Ledvina M. Preparation and isolation of dityrosine. Prep Biochem 1979;9:273–80.
[15] Malencik DA, Sprouse JF, Swanson CA, Anderson SR. Dityrosine: preparation, isolation, and analysis. Anal Biochem 1966;242:202–13.
[16] Boguta G, Dancewicz AM. Formation of dityrosine in aqueous solution of tyrosine exposed to ionizing radiation. Stud Biophys 1979;73:149–56.
[17] Boguta G, Dancewicz AM. Radiation-induced dimerization of tyrosine and glycyltyrosine in aqueous solutions. Int J Radiat Biol 1981;39:163–74.
[18] Narayanama JMR, Stephenson CRJ. Visible light photoredox catalysis: applications in organic synthesis. Chem Soc Rev 2011;40:102–13.
[19] Prier CK, Rankic DA, MacMillan DW. Visible light photoredox catalysis with transition metal complexes: applications in organic synthesis. Chem Rev 2013;113:5322–63.
[20] Ghosh I, Marzo L, Das A, Shaikh R, König B. Visible light mediated photoredox catalytic arylation reactions. Acc Chem Res 2016;49:1566–77.
[21] Silva E, Godoy J. Riboflavin sensitized photooxidation of tyrosine. Intern J Vit Nutr Res 1994;64:253–6.
[22] Pfleiderer W. In: Ayling JE, Nair MG, Baugh CM, editors. Chemistry and biology of pteridines and folates. New York: Plenum Press; 1993. p. 1–16.
[23] Kappock TJ, Caradonna JP. Pterin-dependent amino acid hydroxylases. Chem Rev 1996;96:2659–756.
[24] Castaño C, Dántola ML, Oliveros E, Thomas AH, Lorente C. Oxidation of tyrosine photoinduced by pterin in aqueous solution. Photochem Photobiol 2013;89:1448–55.
[25] Castaño C, Lorente C, Martins-Froment N, Oliveros E, Thomas AH. Degradation of α-melanocyte-stimulating hormone photosensitized by pterin. Org Biomol Chem 2014;12:3877–86.
[26] Castaño C, Vignoni M, Vicendo P, Oliveros E, Thomas AH. Degradation of tyrosine and tryptophan residues of peptides by type I photosensitized oxidation. J Photochem Photobiol B Biol 2016;164:226–35.
[27] Thomas AH, Lorente C, Roitman K, Morales MM, Dántola ML. Photosensitization of bovine serum albumin by pterin: a mechanistic study. J Photochem Photobiol B Biol 2013;120:52–8.
[28] Thomas AH, Zurbano BN, Lorente C, Santos J, Roman EA, Dántola ML. Chemical changes in bovine serum albumin photoinduced by pterin. J Photochem Photobiol B Biol 2014;141:262–8.
[29] Reid LO, Roman EA, Thomas AH, Dántola ML. Photooxidation of tryptophan and tyrosine residues in human serum albumin sensitized by pterin: a model for globular protein photodamage in skin. Biochemistry 2016;55:4777–86.
[30] Monópoli VD, Thomas AH, Capparelli AL. Kinetics and equilibrium study of nickel(II) complexation by pterin and 6-carboxypterin. Int J Chem Kinet 2000;32:231–7.
[31] Eaton DF. In: Scaiano JC, editor. Handbook of organic photochemistry. Boca Raton, Florida: CRC Press; 1989 [chapter 8].
[32] Meech SR, Phillips D. Photophysics of some common fluorescence standards. J Photochem 1983;23:193–217.
[33] Serrano MP, Lorente C, Borsarelli CD, Thomas AH. Unraveling the degradation mechanism of purine nucleotides photosensitized by pterins: the role of charge-transfer steps. ChemPhysChem 2015;16:2244–52.
[34] Murov SL, Carmichael I, Hug GL. Handbook of photochemistry. second ed. New York: Marcel Dekker Ed.; 2009.
[35] Bensasson RV, Land EJ, Truscott TG. Flash photolysis and pulse radiolysis. Contributions to the chemistry of biology and medicine. Oxford: Pergamon Press; 1983. p. 93–120 [chapter 4].
[36] Harriman A. Further comments on redox potentials of tryptophan and tyrosine. J Phys Chem 1987;91:6102–6.
[37] Song Q-H, Hwang KC. Direct observation for photophysical and photochemistry processes of folic acid in DMSO solution. J Photochem Photobiol A 2007;185:51–6.
[38] Harms GS, Pauls SW, Hedstrom JF, Johnson CK. Fluorescence and rotational dynamics of dityrosine. J Fluoresc 1997;7:283–92.
[39] Mahamoud SF, Bialkowski SE. Laser-excited fluorescence of dityrosine. Appl Spectrosc 1995;49:1669–76.
[40] Andersen SO. Characterization of a new type of cross-linkage in resilin, a rubber like protein. Biochim Biophys Acta 1963;69:249–62.
[41] Lehrer SS, Fasman GD. Ultraviolet irradiation effects in poly-L-tyrosine and model compounds. Identification of bityrosine as a photoproduct. Biochemistry 1967;6:757–67.